GUIDANCE AND CONTROL FOR D-SEND#2

Jun'ichiro Kawaguchi*, Tetsujiro Ninomiya*, Hirokazu Suzuki*
***Japan Aerospace Exploration Agency**
kawaguchi.junichiroh@jaxa.jp; ninomiya.tetsujiro@jaxa.jp; suzuki.hirokazu@jaxa.jp

Keywords: *Flight Control, Supersonic Flight, UAV, Dynamic Inversion*

Abstract

This paper describes the current development status of the guidance and control law for D-SEND#2, a supersonic flight test scheduled next year in Sweden to validate JAXA's proprietary low-boom configuration. D-SEND#2 features a balloon-based flight experiment system with an unpowered low-boom demonstrator called the silent supersonic concept model (S3CM). The goal of the guidance and control law is to guide S3CM autonomously to the boom measurement system (BMS), a captive blimp with aerial microphones installed for acoustic data acquisition, and to realize a target flight condition so that the acoustic measurement requirements will be satisfied when the sonic boom reaches the BMS. Challenges lies in developing the guidance and control law: reference trajectory generation regardless of the initial release point, accurate attitude control covering a broad flight envelope, and sufficient robustness in the presence of uncertainties and turbulence. Parametrization and optimization of the reference trajectory, the guidance and control law based on the hierarchy-structured dynamic inversion (HSDI), and robustness evaluation through Monte Carlo simulations (MCS) are elaborated on in this paper to cope with these technical challenges.

1 Introduction

International Civil Aviation Organization (ICAO) has been making an attempt to set up an international standard on sonic boom intensity to permit civil supersonic flight over land. JAXA has been contributing to this attempt by organizing a project team for a drop test for simplified evaluation of non-symmetrically distributed sonic boom (D-SEND). The goal of D-SEND project is to validate JAXA's proprietary low-boom configuration obtained computationally by multidisciplinary design exploration method [1]. D-SEND project consists of two balloon-based flight tests as illustrated in Fig.1: a preliminary campaign (D-SEND#1) to ensure the feasibility of acoustic data acquisition by the boom measurement system (BMS) using two different axisymmetric bodies, followed by the final campaign (D-SEND#2) to demonstrate the low-boom configuration using the silent supersonic concept model (S3CM), whose geometry is given in Fig.2. Both flight tests are conducted at Esrange test range in Sweden supported by the Swedish Space Corporation (SSC) balloon launch team. D-SEND#1 was successfully carried out on May 7th and 16th in 2011 and the results of the flight test are published on [2].

In D-SEND#2 scheduled in summer in 2013, S3CM is released from a stratospheric balloon at the altitude of between 26km to 30km, accelerated by gravity to supersonic region, and autonomously guided to above BMS. BMS records the acoustic data of the reduced sonic boom with not only low-frequency microphones on the ground but also several aerial microphones vertically aligned on the tether hung from the blimp floating 1250m above the ground in order to avoid the influence of the atmospheric turbulence. Flight termination command is transmitted to S3CM immediately after the boom mea-

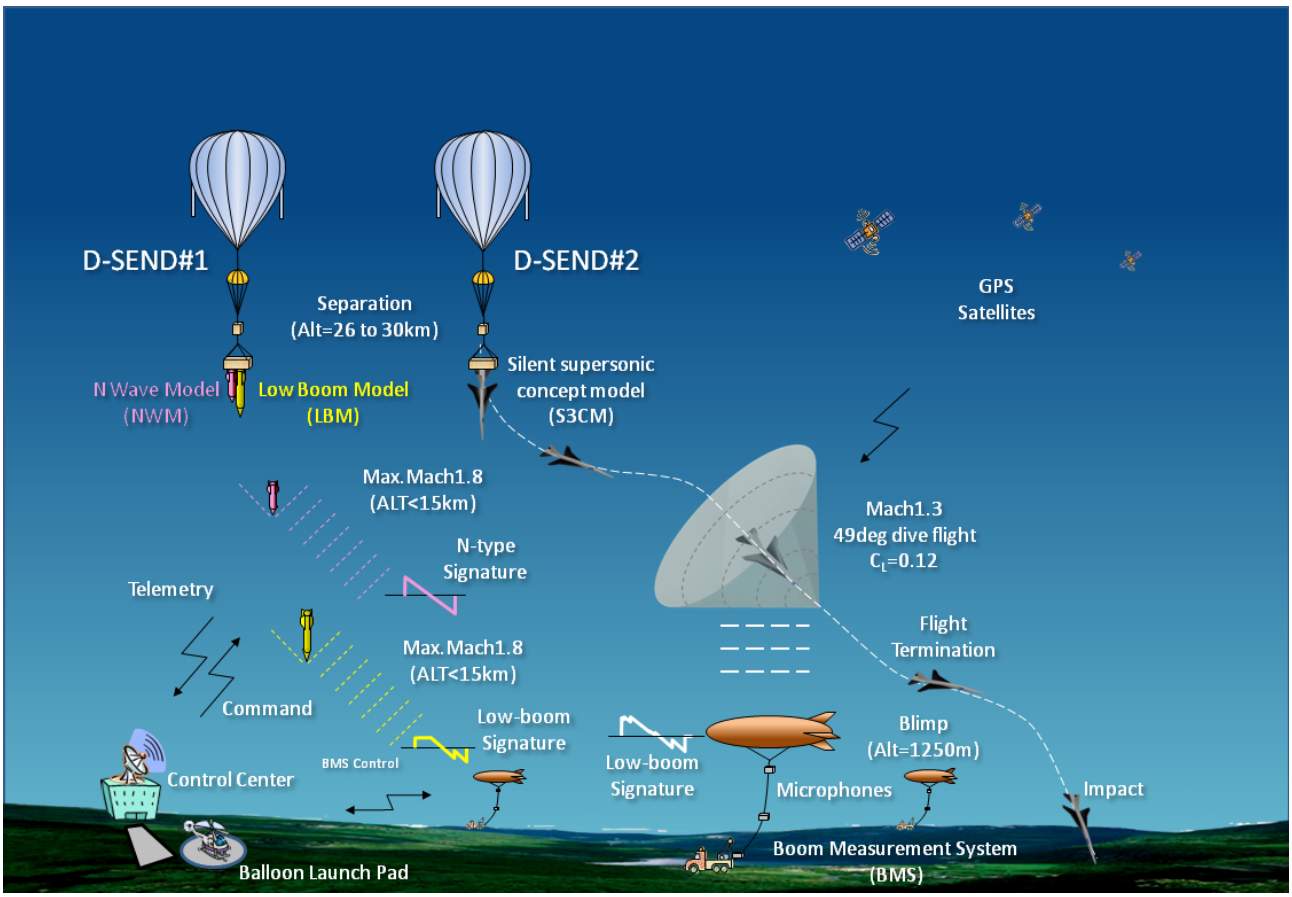

Fig. 1 Outline of the flight expements in D-SEND project

Fig. 2 Silent supersonic concept model (S3CM)

Fig. 3 Quiet supersonic tranport (QSST) concept

surement is finished in order to prevent S3CM from getting into the prohibited area. The low-boom configuration is validated only when S3CM maintains a particular mach number and lift coefficient for a certain period of time and the sonic boom generated during the target flight condition propagates directly to BMS. The target flight condition is defined to simulate the low-boom characteristics of the quiet supersonic transport (QSST) in the cruise flight at Mach 1.6 at the altitude of 14km. The concept image of QSST is shown in Fig.3. Although S3CM, which is not equipped with any thrusters but only a pair of stabilators, is not able to maintain a cruise flight at a constant altitude, the target flight condition can be defined alternatively as a gliding

flight with appropriate combination of altitude and flight path angle. From the viewpoint of flight control, it is challenging to control the four variables (M, C_L, γ, h) at the same time using the only one control input (δ_s). Moreover, S3CM is not separated from the stratospheric balloon at the uniquely determined position. Therefore it is also a challenging problem to develop such a trajectory generation algorithm that maximizes reachability to BMS from the varying initial position and realizes the target flight condition for successful low-boom measurement.

In this paper, the current development status of the guidance and control law for D-SEND#2 is reported. First, the target flight condition is defined where the reduced sonic boom can be most effectively measured at BMS. Then, parametrization and optimization of the trajectory generation algorithm from separation to the target flight condition is performed using the two degrees of freedom (2DOF) longitudinal aircraft dynamics model and the downhill simplex method. After that, the guidance and control law is developed based on the hierarchy-structured dynamic inversion (HSDI), which is based on the time scale separation technique [3]. Finally, robustness of both the trajectory generation algorithm and the HSDI-based flight control law is statistically evaluated through Monte Carlo simulations (MCS) using the six degrees of freedom (6DOF) aircraft dynamics model.

2 Definition of the target flight condition

2.1 Equivalent altitude

The low-boom characteristics of QSST in the level cruise flight can be simulated with S3CM in the gliding flight by setting the ratio between the body length and the equivalent altitude equal to that of QSST. Fig.4 gives the schematic definition of the equiavent altitude. Note that $H = h - h_{mic}$ when $\gamma = 0$. Although the ratio $H/L \approx 300$ for QSST, it is difficult for S3CM to achieve the same H/L due to the excessive dynamic pressure, which has critical effects on the structure and actuators. Computational boom propagation

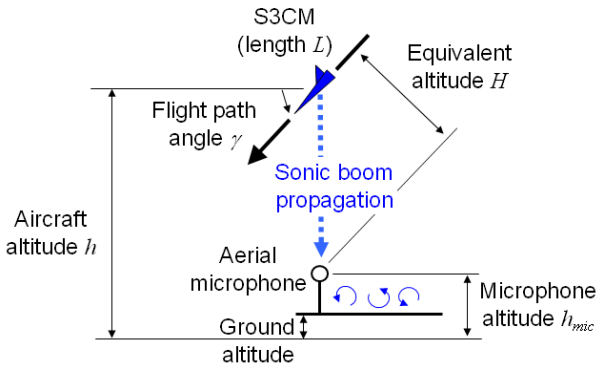

Fig. 4 Definition of equivalent altitude

analysis has shown that the low-boom characteristics can be validated even with $H/L \approx 600$. The analysis has also claimed that Mach number does not have much effect on the boom intensity. Therefore the target Mach number is reduced from $M = 1.6$ to $M = 1.3$.

2.2 Target flight condition

Table 1 shows the boom measurement requirements and flight constraints in D-SEND#2. Although it is required during the boom measurement phase that S3CM is in the gliding flight with constant M and C_L, such a steady flight condition is not physically realized due to decreasing altitude. When constant C_L is achieved by maintaining the angle of attack α, the lift force L increases with decreasing altitude followed by steady pull-up. This results in the loss of M due to increasing drag. On the other hand, constant M is achieved by accelerating S3CM by pull-down maneuver, which involves decreasing C_L, due to increasing sonic speed with decreasing altitude. Therefore, the target flight condition is defined as the following pseudo-steady state: S3CM is accelerated from a low speed to the target M by pull-down maneuver and then increases α to achieve $C_L = 0.12$. S3CM maintains the constant C_L by steady pull-up and M decreases gradually. Fig.5 is the $h - \gamma$ diagram where the isomach line, the H/L contours and the flight requirements listed in Table 1 are indicated. Note that the equivalent airspeed V_{EAS} and the load factor N_z in Fig.5 are reached at the end of the measurement phase.

Table 1 Flight requirements and constraints

Item	Requirement / Constraint	Unit
C_L	0.12	-
M	1.25 to 1.35	-
$\dot{M}$	± 0.01	1/s
H/L	≤ 600	-
N_z	± 4.5	G
V_{EAS}	≤ 360	m/s
Elevation	≥ 3	deg

The most effective acoustic measurement condition is such that the sonic boom propagates vertically to the BMS, which is realized when $\cos^{-1}(1/M) - \gamma = \pi/2$. The target flight condition is thus set at $h = 7.79$km, $\gamma = -49$deg, $M = 1.3$, and $C_L = 0.12$, taking account of the safety margin of 1G for N_z and 10% for V_{EAS}.

3 Flight trajectory generation

3.1 Flight phase

Flight trajectory generation for D-SEND#2 is a two-point boundary value problem from separation to the target flight condition. It is challenging in the sense that both the initial condition and the target BMS are not determined until separation from the stratospheric balloon. Numerical solvers which resort to iteration are not employed because they are time-consuming and solvability is not guaranteed. The flight trajectory generation algorithm for D-SEND#2 is thus developed based on the design policy that the flight trajectory is divided into several flight phases, in each of which design parameters are adjusted for a varying flight range. The following six flight phases are considered:

1. Acceleration and initial roll control
2. Pull-up maneuver
3. Glide flight for range and heading adjustment

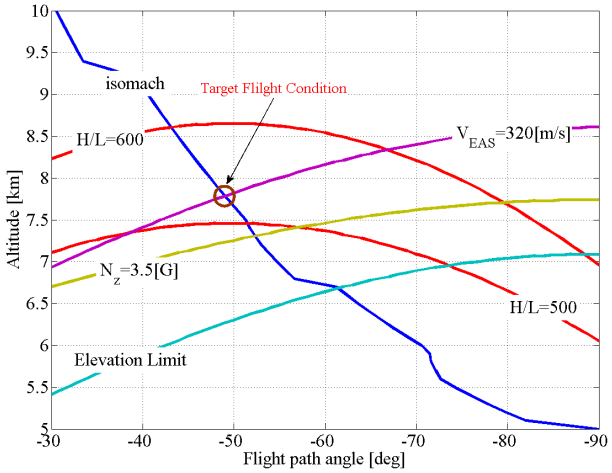

Fig. 5 Definition of target flight condition

4. Dive maneuver for re-acceleration
5. Measurement at the target flight condition
6. Flight termination

Initial roll control in phase 1 initiates immediately after the dynamic pressure becomes large and attitude control using the aerodynamic surfaces is enabled so that the tail of S3CM will point the direction of BMS. Initial roll control, if ideally performed, restricts the aircraft motion in the vertical plane and therefore greatly simplifies the problem.

3.2 Parametrization and optimization

In the following analysis, 2DOF longitudinal aircraft dynamics is employed assuming that initial roll control is ideally performed in phase 1.

3.2.1 Maximization of reachability to BMS

The flight trajectory is characterized by G_{DP1}, G_{GM2}, G_{CM2}, and G_{Nz2} defined in Table 2. The parameters are optimized by the downhill simplex method [4] to achieve the maximum and minimum flight range, in other words, to maximize reachability to BMS. Note that G_{CM2} is excluded from optimization to avoid the gliding flight in the vicinity of $M = 1.0$, where the uncertainties of the aerodynamic characteristics are prominent, and is thus subjected to parametric study.

Table 2 Design parameters for optimization

Phase	Swithing condition	Flight Details
1	$q \geq G_{DP1}$	Vertical acceleration with $\alpha = -4.5$deg
2	$\gamma \geq G_{GM2}$	Pull-up maneuver with up to $\alpha = 12$deg
3	$M \leq G_{CM2}$	Gliding flight at 0.88G
4	$H \leq 11.093$km	Dive maneuver with $N_z = G_{NZ2}$
5	$M \leq 1.25$	Maintain $C_L = 0.12$

Table 3 Optimization results

Parameters	Max. range	Min. range	Unit
G_{DP1}	175.4	7065.2	Pa
G_{CM2}	1.193	1.306	-
G_{NZ2}	-2.603	-3.139	G
G_{GM2}	-8.0	-1.0	deg
Range	31.38	18.60	km

The optimization results are given in Table 3. The 2DOF dynamics model assumes a non-rotating spherical earth and the local atmospheric model in August at Esrange test range is employed. The local steady wind is not considered in the analysis. The atmospheric model is obtained from the monthly NOAA observation data for the last 10 years [5]. The dynamics of α is modeled as combination of the first-order delay with time constant of 1.28 seconds and the delay element of 0.6 seconds. The initial condition is such that $h = 30$km, $V_{EAS} = 0$m/s, and $\gamma = 0$deg. Fig.6 is the time history of α for the maximum and minimum flight range. Fig.6 suggests that the initial roll control be finished within no more than 15 seconds. The maximum flight range is thus limited to 26.0km to guarantee sufficient amount of time for the initial roll control without affecting reachability to BMS. Fig.7 is the $h-M$ diagram where the restrictions regarding V_{EAS} and the structural flutter are indicated.

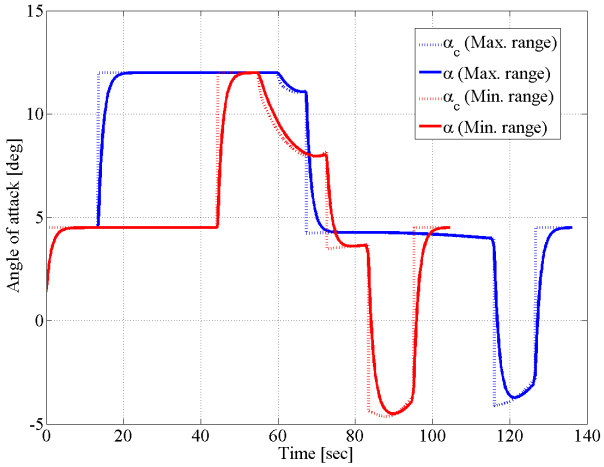

Fig. 6 Time history of α after optimization

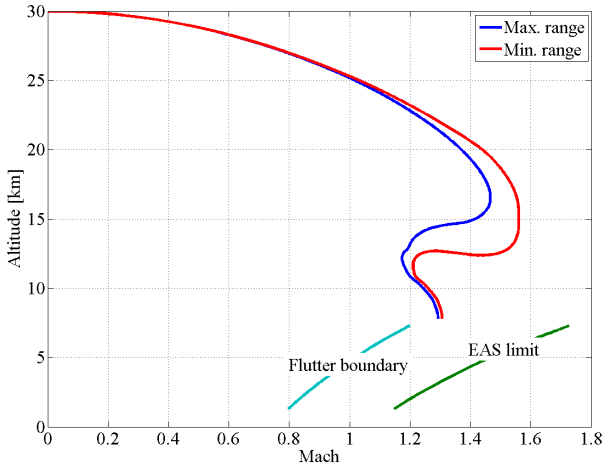

Fig. 7 $h-M$ diagram after optimization

3.2.2 Adjustment for varying range

The optimization scheme in the previous section is similarly performed for some mid flight ranges between 18.6km and 26.0km. The optimization

Table 4 Alternative switching condition

	Min. range	21km	24km	Max. range	Average	Unit
Distance to BMS at the end of phase 3	5.800	5.776	5.703	5.802	5.770	km
Flight range during phase 4	3.845	3.812	3.726	3.885	3.810	km

Table 5 Parameters to switch the flight phase

Phase	Switching condition
1	$q \geq G_{DP1}$
2	$\gamma \geq G_{GM2}$
3	5.770km to BMS
4	$f(h, V_{EAS}, \gamma) \leq 1$
5	$M \leq 1.25$

results for G_{DP1}, G_{GM2}, and their least square approximation are given in Fig.8, which suggests that G_{DP1} and G_{GM2} can be expressed by the linear function with respect to the flight range. It is found, on the other hand, that the least square approximation is not suitable for G_{CM2} and G_{Nz2}. Table 4 indicates that the initial flight range to go has almost nothing to do with the remaining distance to BMS at the end of the gliding flight. It is thus considered as a reasonable parameter to switch phase 3 to phase 4. G_{Nz2} and the switching altitude to phase 5 are obtained using the interface plane $f(h, V_{EAS}, \gamma) = 1$. It is the set of the initial values for h, V_{EAS}, and γ at the beginning of phase 5 which eventually realize the target flight condition. G_{Nz2} is subjected to online parametric study just before the dive maneuver initiates to obtain the reachable initial condition on the interface plane.

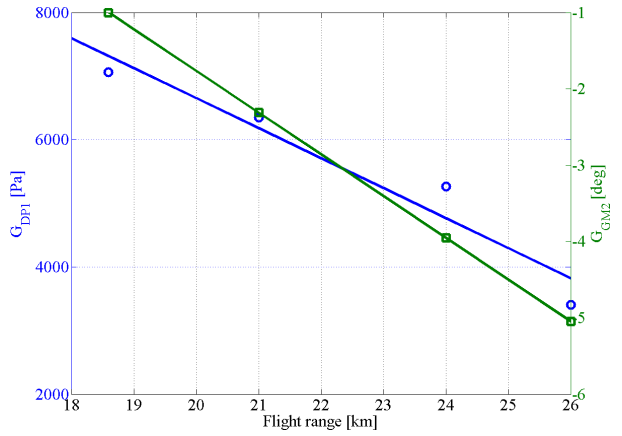

Fig. 8 Optimized parameters for mid flight range

4 Guidance and control law

The guidance and control law for D-SEND#2 is based on HSDI in order to cover the broad flight envelope from the subsonic to supersonic region without rigorous gain scheduling. The HSDI-based flight control law for D-SEND#2 is evaluated for the nominal case without any uncertainties and external turbulence.

4.1 Hierarchy-structured dynamic inversion

An HSDI-based flight control law is developed in such a way that a general fixed-wing aircraft system is decomposed into subsystems according to the time scales inherent in the dynamics and nonlinear dynamic inversion (NDI) is applied to each subsystem. In each subsystem, the *slow* variables are controlled by taking the *fast* variables as fictitious control input. HSDI therefore features a simple nested structure of the following first order NDI controllers.

(1_{st} Layer)

$$V_c = R + \left(\frac{\partial f_R}{\partial V}\right)^{-1} \{-f_R + K_R(R_c - R)\} \quad (1)$$

(2_{nd} Layer)

$$\Theta_c = V + \left(\frac{\partial f_V}{\partial \Theta}\right)^{-1} \{-f_V + K_V(V_c - V)\} \quad (2)$$

Table 6 Interface variables

Phase	1	2	3	4	5
Variable	θ	γ	γ	N_z	N_z

(3_{rd} Layer)

$$\Omega_c = \Omega + \left(\frac{\partial f_\Theta}{\partial \Omega}\right)^{-1} \{-f_\Theta + K_\Theta(\Theta_c - \Theta)\} \quad (3)$$

(4_{th} Layer)

$$\delta_c = \delta + \left(\frac{\partial f_\Omega}{\partial \delta}\right)^{-1} \{-f_\Omega + K_\Omega(\Omega_c - \Omega)\} \quad (4)$$

f_R is the position dynamics in the slowest timescale, f_V is the velocity dynamics in the slow time scale, f_Θ is the attitude dynamics in the fast time scale, and f_Ω is the angular rate dynamics in the fastest time scale. K_R, K_V, K_Θ, and K_Ω are the proportional feedback gain matrices.

4.2 Application to D-SEND#2

4.2.1 Interface variables

The interface variables between the trajectory generation algorithm and the HSDI-based guidance and control law are the pitch angle θ, or N_z, or γ depending on the flight phase as defined in Table 6. θ and N_z belongs to the 3_{rd} layer, and γ belongs to the 2_{nd} layer. Note that N_z is not controlled by taking q as the fictitious control input due to the excessive computational load but the pitch rate command q_c is generated using the conventional PID. q_c is then employed for the HSDI flight control aw for the 4_{th} layer. For the lateral guidance and control, ϕ and β are employed to adjust the heading angle to the target BMS and to maintain the coordinated flight condition ($\beta = 0$).

4.2.2 Initial roll control

Initial roll control for D-SEND#2 is performed in the vicinity of the singular point of $\theta = -90$deg. In order to avoid singularity, the tail direction angle ψ_F is controlled so that ψ_F will point the direction of the target BMS. However, applying HSDI for the initial roll control requires too much computational resources to be implemented. Therefore, the initial roll controller is designed with the conventional PID technique.

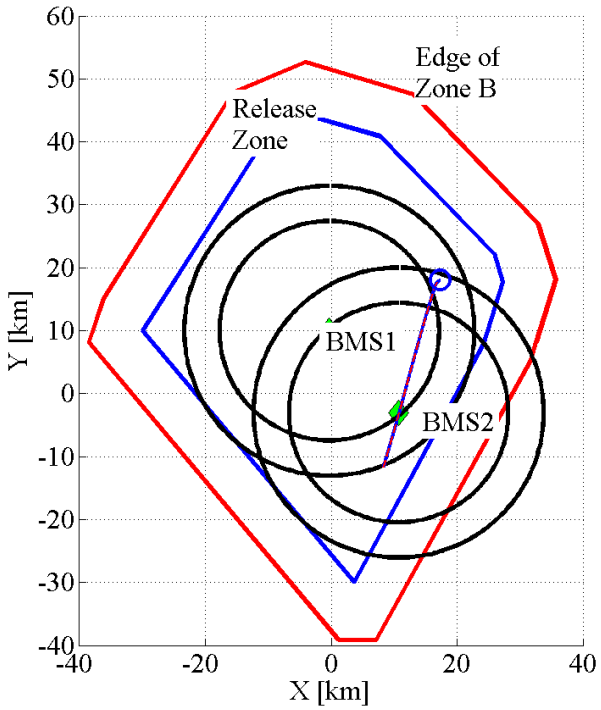

Fig. 9 Simulated nominal flight path

4.2.3 Simulation results

A numerical simulation is performed using the 6DOF nonlinear simulation model to evaluate the control performance for the nominal case. The initial flight range to go and separation altitude are set at 22km and 30km, respectively. The local steady wind model at Esrange test range for August is considered in the analysis. Fig.9 illustrates the simulated flight path and suggests that the initial roll control and the heading angle adjustment are performed with high accuracy. Fig.10 is the $h-M$ diagram and time histories for the variables used in the 6DOF analysis and the measurement requirements in Table 1 are all satisfied.

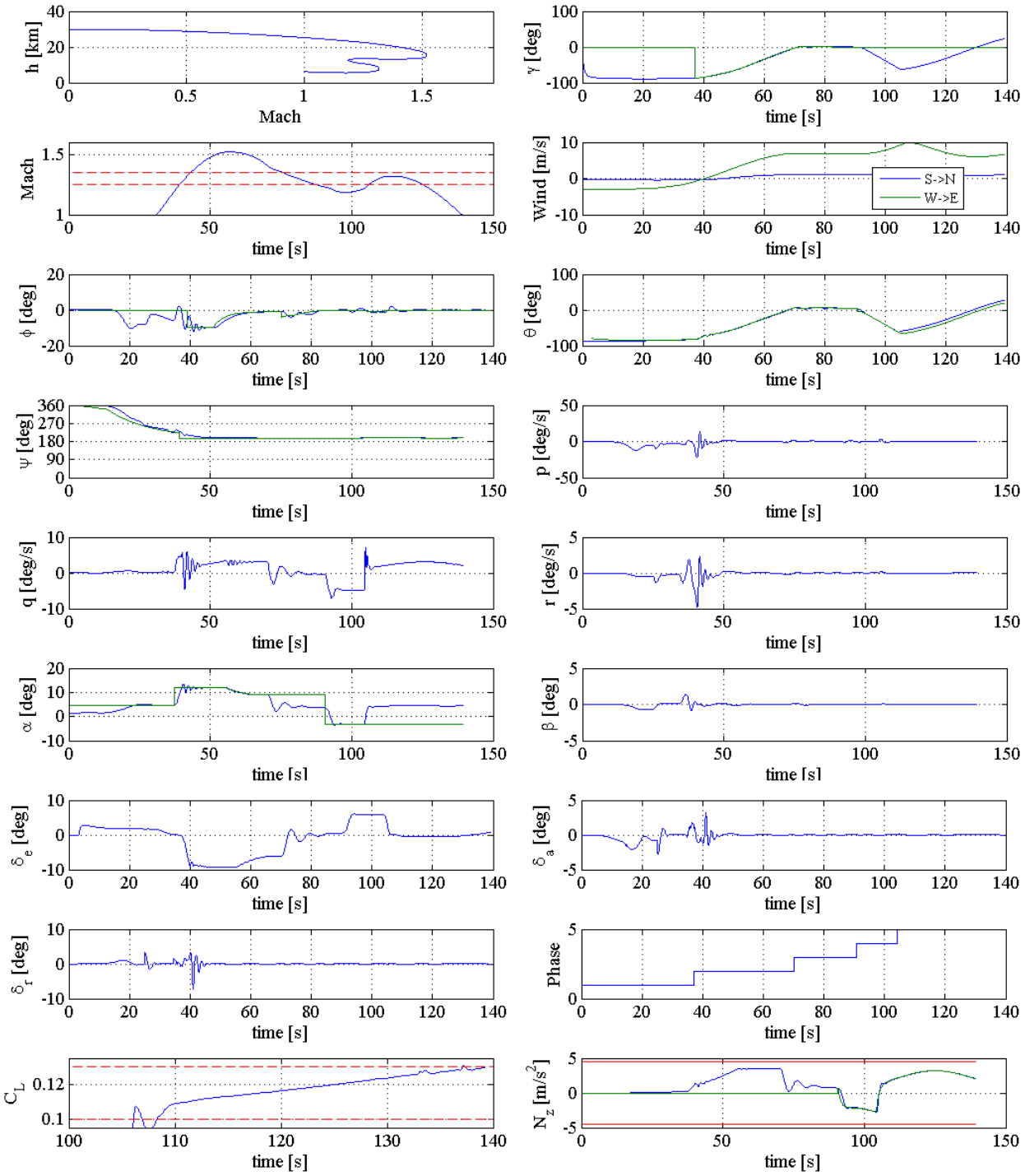

Fig. 10 Time histories for the nominal case

4.3 Robustness evaluation

The robustness evaluation is conducted through MCS with 200 repetitions, where all the uncertain parameters and external disturbances are taken into account simultaneously. The MCS results are characterized by the binomial distribution with the following probability of failure.

$$P_{\text{fail}} = \frac{\sum_{i=1}^{N_{\text{MCS}}} (1 - z_i)}{N_{\text{MCS}}} \tag{5}$$

where N_{MCS} is the number of repetitions and z_i is the mission failure index, i.e. $z_i = 0$ in the case of failure, and $z_i = 1$ in the case of success.The failure cases are categorized into the following three groups:

1. Flight failure

   Unable to maintain a stable flight due to divergence of the attitude dynamics or flight over the prohibited area

2. Violation of the flight restriction

   Flight restrictions for such as N_z, α and β are violated during the simulation

3. Mission failure

   Measurement failure at the target BMS in spite of the stable flight without violating any restrictions.

The MCS results are given in Table 7. Sonic boom propagation is simply modeled in the vertical plane to reduce the computational load. The deviation of the sonic boom from the BMS is defined as the distance from the straight line created by connecting the initial and final points which the sonic boom sweeps during the measurement phase. It is found that all the flight failure is triggered by the failure of the initial roll control and the mission failure occurs mainly because the sonic boom does not reach the BMS also due to the same reason. The results of the MCS robustness evaluation therefore suggests that the parameters for the initial roll control be modified. Then, the design parameters in the trajectory generation algorithm and the HSDI flight control law will be subjected to stochastic parameter optimization to minimize the probability of failure.

Table 7 MCS results

Category	Case	Probability
Success	169	84.5%
Mission failure	21	10.5%
Violation	7	3.5%
Flight failure	3	1.5%
Total	200	$P_{\text{fail}} = 0.155$

5 Conclusions

This paper elaborated on the guidance and control law for S3CM, the unpowered demonstrator in D-SEND#2. The target flight condition to be achieved for successful low-boom measurement was first defined as the pseudo-steady gliding flight. Parametrization and optimization of the flight trajectory was performed to maximize reachability to BMS and adapt a varying flight range. The guidance and control law to track the flight trajectory was finally developed with HSDI. Control performance of the HSDI-based guidance and control law was evaluated through a 6DOF nonlinear simulation and satisfactory results were obtained. Robustness evaluation results through MCS were also satisfactory and offered the clue to further improve the control performance.

References

[1] Chiba, K., Makino, Y., and takatoya, T., "Multidisciplinary Design Exploration of Wing Shape for Silent Supersonic Technology Demonstrator," AIAA Paper 2007-4168, 2007.

[2] http://d-send.jaxa.jp/d_send_e/index.html

[3] Kawaguchi, J., Ninomiya, T., Miyazawa, T., "Stochastic Approach to Robust Flight Control Design Using Hierarchy-Structured Dynamic Inversion, " Journal of Guidance, Control, and Dynamics, Vol. 34, Number 5, ppp.1573-1576, 2011

[4] Press, W. H., Teukolsky, S. A., Vetterling, W. T., and Flannery, B. P., Numerical Recipes in C, 2nd ed., Cambridge Univ. Press, Cambridge, England, 1992

[5] http://www.esrl.noaa.gov/psd/

Copyright Statement